Journal of Materials Chemistry A

COMMUNICATION

View Article Online
View Journal | View Issue

Cite this: J. Mater. Chem. A, 2018, 6, 17307

Received 28th June 2018
Accepted 14th August 2018

DOI: 10.1039/c8ta06195e

rsc.li/materials-a

A building block exchange strategy for the rational fabrication of *de novo* unreachable amino-functionalized imine-linked covalent organic frameworks†

Hai-Long Qian, [abc] Yang Li[d] and Xiu-Ping Yan *[abc]

We show a facile building block exchange strategy for the preparation of amino-functionalized imine-linked covalent organic frameworks (COFs) due to its great significance for promoting the diverse applications of COFs, which are usually inaccessible *via de novo* methods. The developed strategy offers a new method for the preparation of *de novo* unreachable COFs.

Covalent organic frameworks (COFs) are crystalline porous organic materials in which organic monomers are networked with covalent bonds based on reticular chemistry.[1–5] Their unique properties encompassing inherent porosity, high stability, low density, accessible modification, and predicable structures give COFs high potential for applications like energy storage,[6,7] catalysis,[8,9] photoconduction,[10,11] sensing[12] and separation.[13,14] As one of the most studied kinds of COF, imine-linked COFs (ICOFs) are fabricated *via* the polymerization of aldehydes and amines.[15,16] Amino groups, which contain lone pairs of electrons, can form hydrogen bonds and are liable for further derivatization. Thus, amino-functionalized materials, such as metal organic frameworks (MOFs), persistent luminescence nanoparticles, quantum dots, carbon nanotubes, and magnetic nanoparticles are prevalent in various emerging areas.[17–21] However, it is a great challenge to prepare *de novo* amino-functionalized ICOFs (ICOFs-NH_2) due to the participation of amino groups in the formation of ICOFs.[22]

Herein, we report a facile building block exchange (BBE) strategy for preparing *de novo* unreachable ICOFs-NH_2. BBE presents various unique features for preparing unreachable MOFs by direct synthesis methods, engineering the pores and introducing the desired functional behavior of MOFs.[23–28] However, so far utilizing BBE for synthesizing unreachable COFs remains mostly unexplored.[29] As a proof of concept, here we show the design of the BBE strategy for the preparation of *de novo* unreachable PTBD-NH_2 and PTPA-NH_2 (Fig. 1).

The BBE strategy started from the solvothermal preparation of two new crystalline ICOFs PTPA and PTBD as the mother COFs *via* the direct condensation of 1,3,5-tris(4-formyl-phenyl) triazine (PT) with 1,4-phenylenediamine (PA) and benzidine (BD), respectively (Fig. 1; ESI†). In our preliminary design, 3,3′-diaminobenzidine (BD-NH_2) and 1,2,4-benzenetriamine (PA-NH_2) were used to displace the PA in PTPA and the BD in PTBD, respectively. However, the same crystal structure between the mother COFs and daughter COFs in this preliminary design led to no obvious change in the main PXRD patterns of the prepared COFs before and after BBE (Fig. S1 and S2, ESI†), so this is unfavorable for the characterization of the BBE process.

To clearly elucidate the feasibility of the proposed BBE methodology, the BBE preparation of daughter COFs with different structures from their mother COFs was designed. We employed BD-NH_2 and PA-NH_2 to displace the PA in PTPA and the BD in PTBD to produce their daughter ICOFs-NH_2, PTBD-NH_2 and PTPA-NH_2, respectively (Fig. 1; ESI†). The concentration of reactant, reaction time and reaction temperature are critical to the BBE process. As for the BBE of PTPA, 1 equivalent (equiv.) and 5 equiv. of BD-NH_2 resulted in the transformation of the crystalline mother COF PTPA to an amorphous polymer (Fig. S3, black and red lines, ESI†). A further increase of BD-NH_2 to 10 equiv. led to a new crystalline product, indicating the completion of the BBE process (Fig. S3, blue line, ESI†). In contrast, only 1 equiv. of PA-NH_2 was sufficient to drive the transformation of PTBD to PTPA-NH_2 (Fig. S4, black line, ESI†). An increase of PA-NH_2 to 2 equiv. resulted in weak crystallinity and a low yield (Fig. S4, red line, ESI†). However, a further increase of PA-NH_2 to 5 equiv. led to no powder formation after BBE.

[a]State Key Laboratory of Food Science and Technology, Jiangnan University, Wuxi 214122, China. E-mail: xpyan@jiangnan.edu.cn; xpyan@nankai.edu.cn

[b]International Joint Laboratory on Food Safety, Jiangnan University, Wuxi 214122, China

[c]Institute of Analytical Food Safety, School of Food Science and Technology, Jiangnan University, Wuxi 214122, China

[d]College of Chemistry, Research Center for Analytical Sciences, Tianjin Key Laboratory of Molecular Recognition and Biosensing, Nankai University, Tianjin 300071, China

† Electronic supplementary information (ESI) available. See DOI: 10.1039/c8ta06195e

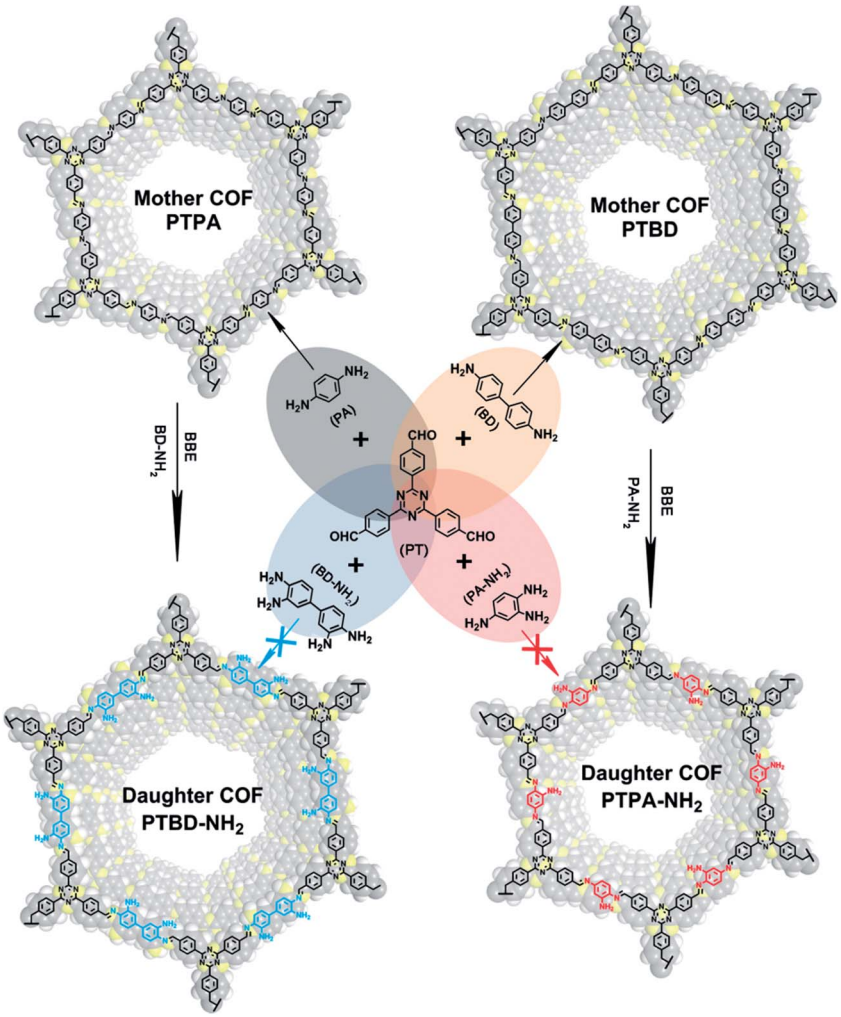

Fig. 1 BBE strategy for the preparation of *de novo* unreachable COFs PTBD-NH_2 and PTPA-NH_2.

One or two days were insufficient for the BBE preparation of PTBD-NH_2 and PTPA-NH_2 due to no obvious diffraction peaks for the obtained powder (Fig. S5 and S6, black and red lines, ESI†). However, a 3 day reaction significantly improved the diffraction peaks of the BBE products, indicating that a long reaction time is beneficial for the BBE process (Fig. S5 and S6, blue lines, ESI†). Expanding the reaction time to 4 days resulted in no obvious change in the diffraction peaks, demonstrating that the replacement of PA and BD by BD-NH_2 and PA-NH_2 was completed in 3 days, respectively (Fig. S5 and S6, magenta lines, ESI†). The optimization of the reaction temperature indicated that a high (80 °C and 120 °C) or low (room temperature) temperature was unsuitable for the BBE process, and 40 °C was the most favorable condition for the BBE preparation of PTBD-NH_2 and PTPA-NH_2 (Fig. S7 and S8, ESI†).

During the BBE process, the color of the mother ICOFs PTPA and PTBD evidently changed from yellow to dark red and tangerine, respectively (Fig. S9 and S10, ESI†). The BBE process from PTPA to PTBD-NH_2 was proved by powder X-ray diffractometry (PXRD). The PXRD pattern of PTPA showed several peaks at 2.90° 4.96°, 7.53°, 9.98°, and 25.89°, which coincided with the simulated pattern for PTPA (Fig. S11–S14, and Table S1, ESI†) produced with the space group *P6/m* ($a = b = 35.58449$ Å, $c = 3.504939$ Å, $\alpha = \beta = 90°$ and $\gamma = 120°$). The BBE process resulted in an obvious change in the PXRD pattern. The obtained daughter COF from PTPA exhibited a PXRD pattern with several peaks at 2.40°, 4.21°, 4.88°, 6.41°, and 25.85° (Fig. 2a), which agreed well with that of the simulated structure of PTBD-NH_2 produced with eclipsed AA stacking mode with the unit cell parameters $a = b = 41.870403$ Å, $c = 3.76792$ Å, $\alpha = \beta = 90°$ and $\gamma = 120°$ (Fig. 2b and c, S15, S16 and Table S2, ESI†).

Similarly, the BBE preparation of PTPA-NH_2 from PTBD was also assessed by PXRD. The diffraction pattern for PTBD showed seven peaks at 2.30°, 4.02°, 6.20°, 8.06°, 8.31°, 10.18° and 25.77°, which was consistent with the simulated PTBD structure (Fig. S17–S20 and Table S3, ESI†). The diffraction peaks of the generated powder after BBE at 2.81°, 4.73°, 5.53°, 7.35° and 25.44° are indexed to the simulated PTPA-NH_2 structure (Fig. 2d–f, S21, S22 and Table S4, ESI†). The significant changes in the PXRD patterns indicated that the structures of PTPA and PTBD were rearranged to form PTBD-NH_2 and PTPA-NH_2 *via* BBE transformation, respectively. Additionally, the

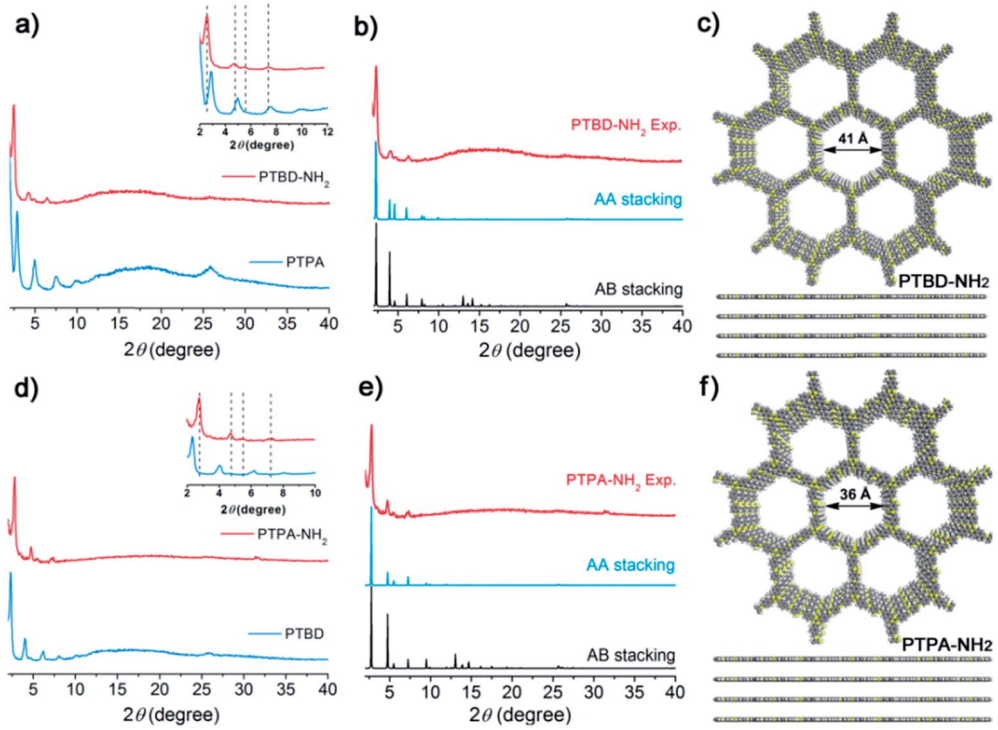

Fig. 2 (a and d) PXRD patterns of the ICOFs before and after BBE. (b and e) Experimental and simulated patterns (AA eclipsed model and AB staggered model) of ICOFs-NH_2. (c and f) Graphic top and side view of ICOFs-NH_2 (gray, C; yellow, N; white, H).

daughter COFs PTBD-NH_2 and PTPA-NH_2, as well as the parent ICOFs PTPA and PTBD, do not conform with the staggered AB model of the simulated structures, indicating that all of the prepared ICOFs have an AA eclipse structure. In contrast, the conventional *de novo* approach is inaccessible for the synthesis of ICOFs-NH_2 PTPA-NH_2 and PTBD-NH_2 as the powders obtained *via* the direct condensation of PT with PA-NH_2 and BD-NH_2 are amorphous polymers rather than crystalline COFs (Fig. S23, ESI†).

The BBE process was also confirmed by Fourier transform infrared (FTIR) spectroscopy, ^{13}C cross-polarization magic angle spinning solid-state nuclear magnetic resonance (CP-MAS SNMR) spectroscopy, elemental analysis, and zeta potential measurements. The FTIR spectra of the BBE product from PTPA show similar vibration bands to that of PTBD, but also show an additional two N–H stretching bands for the –NH_2 groups (3411 cm^{-1}, stretching of one N–H overlaid with the N–H stretching of incompletely reacted groups at the defects; 3197 cm^{-1}, stretching of the other N–H), indicating the successful conversion of PTPA to PTPB-NH_2 (Fig. 3a, S24 and S25, ESI†). The BBE product of PTBD also exhibited similar vibration bands to that of PTPA and an additional two N–H stretching bands (3418 cm^{-1}, 3170 cm^{-1}), confirming the transfer from PTBD to PTPA-NH_2 (Fig. 3d). ^{13}C CP-MAS SNMR spectroscopy offers more strong evidence for BBE. Compared with the CP-MAS-SNMR spectra of the original PTPA, great changes were observed after the BBE process. In addition to the peak of 164 ppm, corresponding to the carbon of the amines, the ^{13}C CP-MAS SNMR spectra of PTBD-NH_2 show a peak at 143 ppm for the carbon of the aromatic amine (Fig. 3b). The BBE of PTBD also led to great changes and the carbon peaks of the amine and aromatic amine shifted to 164 ppm and 146 ppm, respectively (Fig. 3c). Additionally, elemental analysis gave the content of C (73.51 ± 2.39%), H (4.78 ± 0.44%), and N (20.15 ± 1.21%) for the as-prepared PTBD-NH_2 *via* BBE, which was in good agreement with the analytically calculated content of C (76.35%), H (4.58%) and N (19.08%) for the simulated infinite PTBD-NH_2. Meanwhile, the measured elemental content (C, 73.73 ± 1.94%; H, 4.67 ± 0.40%; N, 20.26 ± 1.16%) for the as-prepared PTPA-NH_2 *via* BBE also coincided with the theoretical values (C, 75.63%; H, 4.33%; N, 20.04%). The zeta potentials of the obtained PTBD-NH_2 (−3.89 mV) and PTPA-NH_2 (−10.63 mV) were less negative than those of PTBD (−32.03 mV) and PTPA (−38.54 mV), respectively, due to the introduction of –NH_2 to the COFs (Fig. S26 and S27, ESI†). All of the above results strongly support the reality of the BBE process.

N_2 adsorption–desorption analysis was used to characterize the pore properties of the prepared ICOFs (Fig. 3c and f). The Brunauer–Emmett–Teller (BET) surface areas and the pore sizes of PTPA and PTBD-NH_2 *via* BBE were calculated to be 579 m^2 g^{-1} and 398 m^2 g^{-1}, and *ca.* 38 Å and 41 Å (Fig. S28 ESI†), respectively. The prepared PTBD and PTPA-NH_2 gave BET surface areas of 605 m^2 g^{-1} and 369 m^2 g^{-1}, and pore sizes of *ca.* 43 Å and 36 Å (Fig. S29 ESI†), respectively. The loss in BET surface area after BBE was a result of the smaller pieces of the obtained ICOF-NH_2 (Fig. S30, ESI†).

The scanning electron microscopy (SEM) and transmission electron microscopy (TEM) images show that the daughters

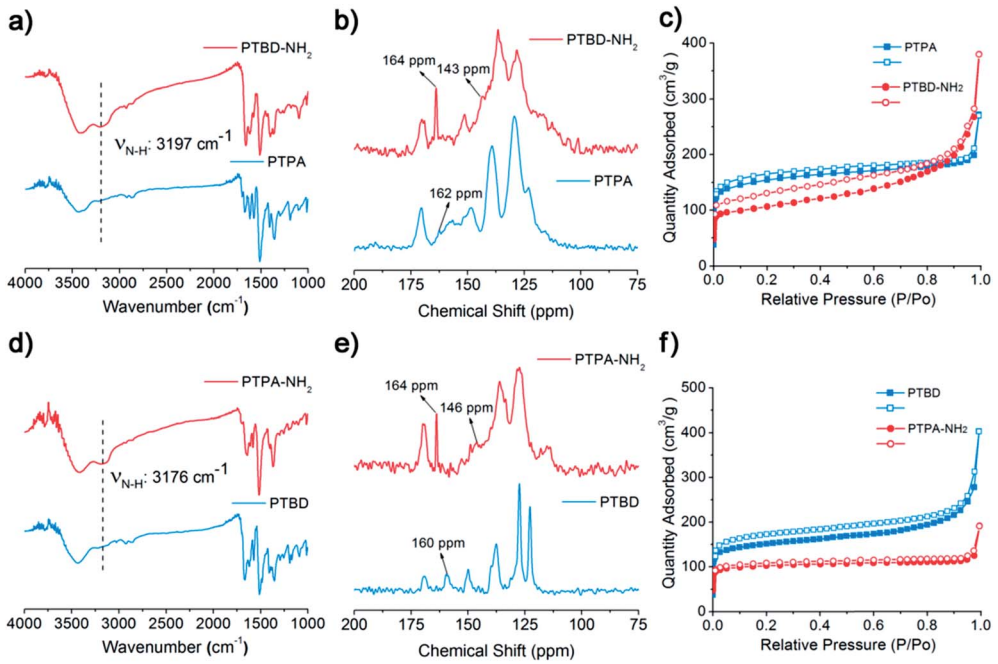

Fig. 3 (a and d) FTIR spectra of the ICOFs before and after BBE. (b and e) ^{13}C CP-MAS SNMR spectra of the ICOFs before and after BBE. (c and f) N_2 adsorption–desorption isotherms for the ICOFs before and after BBE.

PTBD-NH_2 and PTPA-NH_2 exhibited obviously different morphologies from their mother COFs PTPA and PTBD, but were similar to PTBD and PTPA, respectively (Fig. S31 and S32, ESI†). Thermogravimetric curves indicated that the as-prepared COFs exhibit high thermal stability with no unusual weight loss up to 400 °C (Fig. S33 and S34, ESI†).

All of the above characterization data have confirmed the successful preparation of ICOFs-NH_2, indicating that BBE is a promising synthetic strategy to resolve the challenge of preparing *de novo* unreachable COFs. The preparation of COFs is on the basis of dynamic covalent chemistry (DCC),[2,30,31] which is also a key mechanism of BBE. Due to the linkage of organic monomers with reversible covalent bonds, the substituting monomers can exchange the building blocks as long as sufficient driving forces are provided.

The formation of ICOFs is based on the nucleophilic addition reaction of aldehydes and amines. Compared with PA, the enhancement of the p–π conjugated system of BD-NH_2 reduces the electronic cloud density of the amino group, leading to BD-NH_2 having a lower nucleophilicity than PA. Therefore, a high concentration (10 equiv.) of BD-NH_2 is required to drive the nucleophilic substitution between the PA in PTPA and BD-NH_2. In contrast, the higher nucleophilicity of PA-NH_2 compared to that of BD results in only 1 equiv. of PA-NH_2 being sufficient to drive the nucleophilic substitution for the preparation of PTPA-NH_2 from PTBD. A further increase in the concentration of PA-NH_2 results in a rapid reaction which is favorable for the formation of amorphous polymers and oligomers.[32] The reversibility of the covalent bonds in COFs results in the repeated formation and breakage of the linkage. The formation of polymers is always alongside the self-healing feedback process which includes "error checking" and "proof-reading", which is a key process for the formation of ordered structures.[30,31] This self-healing feedback needs sufficient time to reduce the incidence of defects in the structure. Therefore, a three day reaction is required to complete the formation of the stable crystalline structure of PTPA-NH_2 and PTBD-NH_2. DCC is a thermodynamically controlled process and the temperature is essential to guarantee the reversibility of the reaction.[2,3] Different from the traditional synthesis of COFs at high temperatures, the BBE process occurs under moderate temperatures. A high temperature leads to high solubility for the reactant and a high reaction rate, which are unsuitable for the replacement reaction.

Conclusions

We have proposed a BBE strategy for the preparation of *de novo* inaccessible COFs. The higher reactivity of the substituting monomers provides sufficient driving force for BBE. In contrast, a higher concentration is needed to drive the BBE process in the case of the substituting monomers with a lower reactivity. Adequate reaction time and suitable reaction temperature are also critical to the BBE process. The proposed strategy not only extends amino-function into COF materials, but also opens up a new way to prepare *de novo* inaccessible functionalized COFs.

Conflicts of interest

The authors declare no conflicts of interest.

Acknowledgements

This work was supported by the National Basic Research Program of China (No. 2015CB932001), the National Natural Science Foundation of China (No. 21775056, 21804055), the China Post-doctoral Science Foundation (No. 2018M630510), the National First-class Discipline Program of Food Science and Technology (No. JUFSTR20180301), and the Fundamental Research Funds for the Central Universities (No. JUSRP11844 and JUSRP51714B).

Notes and references

1 A. P. Côté, A. I. Benin, N. W. Ockwig, M. O'Keeffe, A. J. Matzger and O. M. Yaghi, *Science*, 2005, **310**, 1166–1170.
2 X. Feng, X. Ding and D. Jiang, *Chem. Soc. Rev.*, 2012, **41**, 6010–6022.
3 S. Y. Ding and W. Wang, *Chem. Soc. Rev.*, 2013, **42**, 548–568.
4 P. J. Waller, F. Gandara and O. M. Yaghi, *Acc. Chem. Res.*, 2015, **48**, 3053–3063.
5 A. G. Slater and A. I. Cooper, *Science*, 2015, **348**, aaa8075.
6 H. Furukawa and O. M. Yaghi, *J. Am. Chem. Soc.*, 2009, **131**, 8875–8883.
7 L. A. Baldwin, J. W. Crowe, D. A. Pyles and P. L. Mcgrier, *J. Am. Chem. Soc.*, 2016, **138**, 15134–15137.
8 S. Y. Ding, J. Gao, Q. Wang, Y. Zhang, W. G. Song, C. Y. Su and W. Wang, *J. Am. Chem. Soc.*, 2011, **133**, 19816–19822.
9 H. Xu, J. Gao and D. Jiang, *Nat. Chem.*, 2015, **7**, 905–912.
10 S. Chandra, T. Kundu, S. Kandambeth, R. Babarao, Y. Marathe, S. M. Kunjir and R. Banerjee, *J. Am. Chem. Soc.*, 2014, **136**, 6570–6573.
11 T. Sick, A. G. Hufnagel, J. Kampmann, I. Kondofersky, M. Calik, J. M. Rotter, A. Evans, M. Doblinger, S. Herbert, K. Peters, D. Bohm, P. Knochel, D. D. Medina, D. Fattakhova-Rohlfing and T. Bein, *J. Am. Chem. Soc.*, 2018, **140**, 2085–2092.
12 S. Dalapati, S. Jin, J. Gao, Y. Xu, A. Nagai and D. Jiang, *J. Am. Chem. Soc.*, 2013, **135**, 17310–17313.
13 X. Han, J. Huang, C. Yuan, Y. Liu and Y. Cui, *J. Am. Chem. Soc.*, 2018, **140**, 892–895.
14 H. L. Qian, C. X. Yang, W. L. Wang, C. Yang and X. P. Yan, *J. Chromatogr. A*, 2018, **1542**, 1–18.
15 J. L. Segura, M. J. Mancheno and F. Zamora, *Chem. Soc. Rev.*, 2016, **45**, 5635–5671.
16 P. J. Waller, S. J. Lyle, T. M. Osborn Popp, C. S. Diercks, J. A. Reimer and O. M. Yaghi, *J. Am. Chem. Soc.*, 2016, **138**, 15519–15522.
17 M. Wang, L. Guo and D. Cao, *Anal. Chem.*, 2018, **90**, 3608–3614.
18 H. Tetsuka, R. Asahi, A. Nagoya, K. Okamoto, I. Tajima, R. Ohta and A. Okamoto, *Adv. Mater.*, 2012, **24**, 5333–5338.
19 J. Shi, X. Sun, J. Zhu, J. Li and H. Zhang, *Nanoscale*, 2016, **8**, 9798–9804.
20 L. Ma, H. L. Zhuang, S. Wei, K. E. Hendrickson, M. S. Kim, G. Cohn, R. G. Hennig and L. A. Archer, *ACS Nano*, 2015, **10**, 1050–1059.
21 M. Chambers, X. Wang, L. Ellezam, O. Ersen, M. Fontecave, C. Sanchez, L. Rozes and C. Mellot-Draznieks, *J. Am. Chem. Soc.*, 2017, **139**, 8222–8228.
22 M. S. Lohse, T. Stassin, G. Naudin, S. Wuttke, R. Ameloot, D. De Vos, D. D. Medina and T. Bein, *Chem. Mater.*, 2016, **28**, 626–631.
23 P. Deria, J. E. Mondloch, O. Karagiaridi, W. Bury, J. T. Hupp and O. K. Farha, *Chem. Soc. Rev.*, 2014, **43**, 5896–5912.
24 O. Karagiaridi, W. Bury, J. E. Mondloch, J. T. Hupp and O. K. Farha, *Angew. Chem., Int. Ed.*, 2014, **53**, 4530–4540.
25 B. J. Burnett, P. M. Barron, C. Hu and W. Choe, *J. Am. Chem. Soc.*, 2011, **133**, 9984–9987.
26 K. Min, J. F. Cahill, Y. Su, K. A. Prather and S. M. Cohen, *Chem. Sci.*, 2011, **3**, 126–130.
27 O. Karagiaridi, M. B. Lalonde, W. Bury, A. A. Sarjeant, O. K. Farha and J. T. Hupp, *J. Am. Chem. Soc.*, 2012, **134**, 18790–18796.
28 O. Karagiaridi, W. Bury, A. A. Sarjeant, C. L. Stern, O. K. Farha and J. T. Hupp, *Chem. Sci.*, 2012, **3**, 3256–3260.
29 C. Qian, Q. Y. Qi, G. F. Jiang, F. Z. Cui, Y. Tian and X. Zhao, *J. Am. Chem. Soc.*, 2017, **139**, 6736–6743.
30 S. J. Rowan, S. J. Cantrill, G. R. Cousins, J. K. Sanders and J. F. Stoddart, *Angew. Chem., Int. Ed.*, 2002, **41**, 898–952.
31 Y. Jin, Q. Wang, P. Taynton and W. Zhang, *Acc. Chem. Res.*, 2014, **47**, 1575–1586.
32 X. Feng, L. Chen, Y. Dong and D. Jiang, *Chem. Commun.*, 2011, **47**, 1979–1981.